Helical configurations of elastic rods in the presence of a long-range interaction potential

2010 J. Phys. A: Math. Theor. 43 085214

(http://iopscience.iop.org/1751-8121/43/8/085214)

IOP PUBLISHING JOURNAL OF PHYSICS A: MATHEMATICAL AND THEORETICAL

J. Phys. A: Math. Theor. **43** (2010) 085214 (19pp) doi:10.1088/1751-8113/43/8/085214

Helical configurations of elastic rods in the presence of a long-range interaction potential

S De Lillo[1,2], G Lupo[1,2] and M Sommacal[1,2]

[1] Dipartimento di Matematica e Informatica and INSTM-Village, Università degli Studi di Perugia, Via Vanvitelli 1, 06123 Perugia, Italy
[2] Istituto Nazionale di Fisica Nucleare, Sezione di Perugia, Perugia, Italy

E-mail: Matteo.Sommacal@pg.infn.it

Received 26 June 2009, in final form 14 December 2009
Published 8 February 2010
Online at stacks.iop.org/JPhysA/43/085214

Abstract
Recently, the integrability of the stationary Kirchhoff equations describing an elastic rod folded in the shape of a circular helix was proven. In this paper we explicitly work out the solutions to the stationary Kirchhoff equations in the presence of a long-range potential which describes the average constant force due to a Morse-type interaction acting among the points of the rod. The average constant force results to be parallel to the normal vector to the central line of the folded rod; this condition remarkably permits to preserve the integrability (indeed the solvability) of the corresponding Kirchhoff equations if the elastic rod features constant or periodic stiffnesses and vanishing intrinsic twist. Furthermore, we discuss the elastic energy density with respect to the radius and pitch of the helix, showing the existence of stationary points, namely stable and unstable configurations, for plausible choices of the featured parameters corresponding to a real bio-polymer.

PACS numbers: 02.30.Ik, 02.30.Zz, 62.20.D−, 81.05.Lg, 87.15−v

(Some figures in this article are in colour only in the electronic version)

1. Introduction

The description of polymers and bio-polymers at different space- and time-scales is a subject of increasing interest in view of their paramount role in several fields of life and material sciences [1–3]. As a matter of fact, atomistic simulations are providing a wealth of results for short-time dynamics of model systems [2, 4, 5]. However, despite the terrific advances of computer power and software efficiency, long-time phenomena such as protein folding or phase transitions remain outside the limits of such approaches. On the other hand, analytical models based on classical elasticity theory [6–8] do not suffer from space or time limitations,

but often involve such an amount of idealization that a direct connection with experiments is lost. In order to fill this gap, we have started a comprehensive research program aimed to provide a direct link between atomistic simulations and analytical models. The first step is the development of a model including the essential features of complex systems such as natural copolymers or proteins, namely shape and elasticity variations along the backbone together with a proper description of long-range steric and specific intra-chain interactions. Reliable treatments of shape and elasticity variations along the chain have been dealt with in the previous studies [9, 10]. Here we will be concerned with the inclusion of long-range interactions and with their tuning effect on the chain characteristics issuing from intrinsic elastic properties. While the overall structure of polymeric materials is further tuned by other specific interactions (e.g. hydrogen bonds, inter-chain and solute–solvent interactions, etc), it is well known that the behavior of several polymers in low-polarity solvents is dominated by the intra-chain short- and long-range interactions included in our model; under these circumstances, the electrostatic effects are negligible. In any case, as shown in [11, 12], a qualitative change in the geometrical configuration of the polymer is not expected when the electrostatic screening is supposed to be uniformly distributed along the chain. These conditions are respected by a large class of synthetic polymers of technological relevance and by many proteins. Clearly, the electrostatic effects cannot be neglected in the case of the DNA (which contains charged phosphates) and of the hydrophobic regions of proteins in physiological conditions.

Proper inclusion of these and other specific interactions requires a deeper understanding of the basic behavior underlying those features. Moreover, temperature and non-homogeneous mechano-chemical properties play no role in our description, e.g. see [13]. As a matter of fact, different helical and/or semi-extended structures can be obtained by simply tuning local elastic properties and long-range steric interactions [1], thus offering a demanding playground for analyzing the reliability of any general model. We show that a qualitative description of some fundamental features of the many molecular systems our model applies to can be achieved through explicit analytical solutions (in the sense of integrable systems) of Kirchhoff equations, without recurring to numerical simulations. This is the reason why we think that the present study can represent a significant step toward a more general and effective treatment of macromolecules of natural and synthetic origin.

In the next section we introduce a long-range interaction in the elastic rod model and then derive the static Kirchhoff equations in the presence of an external force in section 3. In section 4 we solve the system of Kirchhoff equations in the case of circular helices, through an inverse problem approach, obtaining the elastic stiffnesses and the explicit components of the external force. Finally sections 5 and 6 are devoted to the example of a specific long-range interaction. We discuss a Morse-type potential and the corresponding energy density landscape of the rod, which shows the appearance of minima configurations for realistic values of the parameters characterizing the interaction.

2. The long-range interaction on a circular helix

We start our analysis by discussing how to describe a long-range interaction among the points of the rod.

In a given reference frame $\mathcal{O}$, let us consider a circular helix parametrized by the vector function $\vec{P} : \mathbb{R} \longrightarrow \mathbb{R}^3$:

$$\vec{P}(t) = \{r \cos t, r \sin t, ct\}, \tag{1}$$

where r is the helix radius and $c = \frac{p}{2\pi}$, p being the pitch. Curve (1) represents the central line of the elastic rod.

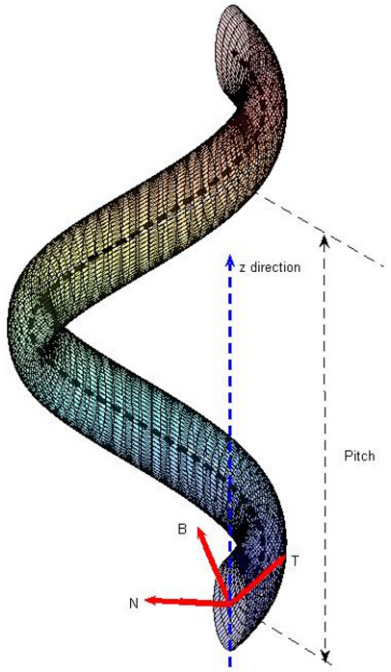

Figure 1. The elastic rod in the circular helix configuration.

Making use of the Frenet relations (see for instance [14]), we can define the *normal* $\vec{N}(t)$, the *binormal* $\vec{B}(t)$ and the *tangent* $\vec{T}(t)$ vectors to the given curve $\vec{P}(t)$ (see figure 1):

$$\begin{aligned}
\vec{N}(t) &= \frac{\dot{\vec{T}}(t)}{|\dot{\vec{T}}(t)|} = \{-\cos t, -\sin t, 0\} \\
\vec{B}(t) &= \vec{T}(t) \times \vec{N}(t) = \left\{ \frac{c \sin t}{\sqrt{c^2+r^2}}, -\frac{c \cos t}{\sqrt{c^2+r^2}}, \frac{r}{\sqrt{c^2+r^2}} \right\} \\
\vec{T}(t) &= \frac{\dot{\vec{P}}(t)}{|\dot{\vec{P}}(t)|} = \left\{ -\frac{r \sin t}{\sqrt{c^2+r^2}}, \frac{r \cos t}{\sqrt{c^2+r^2}}, \frac{c}{\sqrt{c^2+r^2}} \right\},
\end{aligned} \tag{2}$$

where $\cdot$ indicates the derivation with respect to the angular parameter t, and $\times$ is the usual cross product between vectors in $\mathbb{R}^3$.

In order to define a proper long-range interaction of the helix, we consider the following force field $\vec{F}^{(\mathrm{long})}(t, t')$ acting between the points $\vec{P}(t)$ and $\vec{P}(t + t')$ of the central line of the rod (see figure 2):

$$\vec{F}^{(\mathrm{long})}(t, t') = \Phi(|\vec{X}(t, t')|) \frac{\vec{X}(t, t')}{|\vec{X}(t, t')|} \tag{3a}$$

$$\vec{X}(t, t') = \vec{P}(t + t') - \vec{P}(t), \tag{3b}$$

where

$$\Phi(x) = -\frac{\mathrm{d}}{\mathrm{d}x} V(x) \tag{4}$$

can be expressed in terms of the derivative of a suitable potential function $V(x)$ (see below).

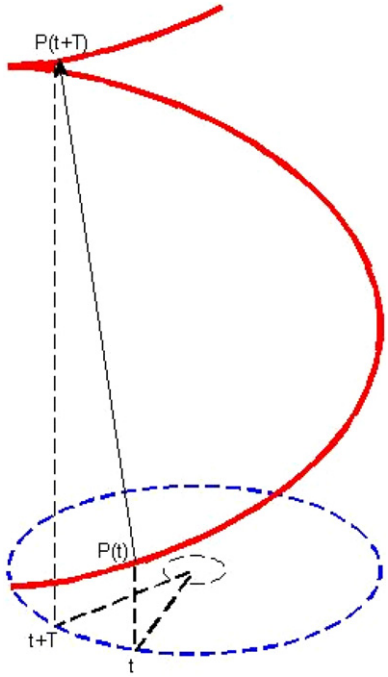

Figure 2. Force field between two points of the helix.

When discussing the long-range interaction force, it is important to observe that we do not take into account the physical dimensions (height and width) of the cross section of the rod, namely we assume that these are negligible with respect to the total arc-length of the rod, placing the force vectors on the centroids of the cross sections (i.e. the intersection between the central line $\vec{P}(t)$ and a section of the rod with a plane perpendicular to $\vec{P}(t)$).

For a circular helix described by (1), we have

$$|\vec{X}(t,t')| \equiv X(t') = \sqrt{2r^2[1-\cos t'] + (ct')^2}, \tag{5}$$

which depends on the angle difference $t' = (t+t') - t$. The three components of the long-range interaction force $\vec{F}^{(\mathrm{long})}(t,t')$ in the fixed reference frame $\mathcal{O}$ are

$$\begin{cases} F_1^{(\mathrm{long})}(t,t') = \dfrac{r[\cos(t+t') - \cos t]}{X(t')}\,\Phi(X(t')) \\ F_2^{(\mathrm{long})}(t,t') = \dfrac{r[\sin(t+t') - \sin t]}{X(t')}\,\Phi(X(t')) \\ F_3^{(\mathrm{long})}(t,t') = \dfrac{ct'}{X(t')}\,\Phi(X(t')). \end{cases} \tag{6}$$

As suggested in [7, 8], for a rod of infinite length whose coarse-grained structure is described by an elastic continuous model, the resultant force $\vec{F}^{(\mathrm{ext})}(t)$ acting on a point $\vec{P}(t)$ of the helix (1) is obtained integrating (6) as $t' \in (-\infty, 0^-) \cup (0^+, \infty)$ and keeping into account the contributions due to the simultaneous interaction of $\vec{P}(t)$ with the points $\vec{P}(t+t')$ and $\vec{P}(t-t')$ (namely we need to perform two 'symmetric' integrations as $t' \in (0^+, \infty)$ and

$t' \in (0^-, -\infty)$):

$$\vec{F}^{(\mathrm{ext})}(t) = \int_{0^+}^{\infty} [\vec{F}^{(\mathrm{long})}(t, t') + \vec{F}^{(\mathrm{long})}(t, -t')]\, \mathrm{d}t', \tag{7}$$

where we assumed that the function $\vec{F}^{(\mathrm{long})}(t, t')$ is continuous in $t' = 0$ and the symbols 0^+ and 0^- have been introduced to avoid the interaction of the point $\vec{P}(t)$ with itself.

On the other hand, for rods of finite length, we do not expect negligible border effects as discussed in [8]. In the following we focus on rods of infinite length, while the problem of rods of finite length will be the subject of future investigation. At this stage, it is worth noting that many natural and synthetic macromolecular systems are a compound of regular regions connected through disordered regions. Thus, a realistic model must necessarily be *piecewise* regular. However, in many cases, the regions characterized by a total regularity (like the α-helices or the β-strands) are so long that it is reasonable to assume their length to be infinite. This is also why, in the present paper, we focus only on helical (and degenerate-helical) configurations, see section 4.

The three components of $\vec{F}^{(\mathrm{ext})}(t)$ in the reference frame $\mathcal{O}$, via (6) and (7), reduce to

$$\begin{cases} F_1^{(\mathrm{ext})}(t) = -\mathcal{F} \cos t \\ F_2^{(\mathrm{ext})}(t) = -\mathcal{F} \sin t \\ F_3^{(\mathrm{ext})}(t) = 0, \end{cases} \tag{8a}$$

where

$$\mathcal{F} = 2r \int_{0^+}^{\infty} \frac{1 - \cos t'}{X(t')}\, \Phi(X(t'))\, \mathrm{d}t'. \tag{8b}$$

By comparing (2) with (8*a*)–(8*b*), we observe that the resultant force $\vec{F}^{(\mathrm{ext})}(t)$ acting on $\vec{P}(t)$ has constant modulus $|\vec{F}^{(\mathrm{ext})}(t)| = |\mathcal{F}|$ and its direction is parallel to the normal vector $\vec{N}(t)$.

It is thus possible to determine the distributed force $\vec{f}(t)$ (i.e. the load) due to the presence of the external force (8*a*), (8*b*), acting on each single point $\vec{P}(t)$. Taking into account the local character of $\vec{F}^{(\mathrm{ext})}(t)$, we recall that the total force applied to a finite portion of the rod $[0, T]$ is obtained by integrating the external force $\vec{F}^{(\mathrm{ext})}(t)$ with respect to the angular parameter $t \in [0, T]$. Then the load is defined as the derivative of the total force with respect to the arc-length s (see [15]),

$$\vec{f}(t) = \frac{\mathrm{d}}{\mathrm{d}s} \int_0^t \vec{F}^{(\mathrm{ext})}(t')\, \mathrm{d}t' = \frac{1}{\sqrt{c^2 + r^2}}\, \vec{F}^{(\mathrm{ext})}(t), \tag{9}$$

considering that $s = t\sqrt{c^2 + r^2}$ as implied by (1). It is worth noting that from (9) it follows that the physical dimensions of the load $\vec{f}$ are $[N/m]$.

3. Kirchhoff equations for elastic rods in the presence of an external force

In this section we resume the main features of the static Kirchhoff model for an elastic rod, see [17, 18]. We follow [9] as a guideline, but we introduce in the model an additional long-range interaction force $\vec{F}^{(\mathrm{ext})}(s)$, see (8*a*) and (8*b*), proving analytically the statements formulated in [8]. This additional force, $\vec{F}^{(\mathrm{ext})}(s)$, can be regarded as an external load (distributed force) acting on all the points of the rod, see (9).

An elastic rod is a deformable three-dimensional object whose length in the longitudinal direction is assumed larger than its length along the transverse direction; while the longitudinal width could be finite or infinite, the transverse one is always finite.

As explained in [9], this model considers deformations of the elastic rod due to bending and torsion and does not allow deformations along the longitudinal direction due to shear, extension and compression.

Let us define a smooth curve in ordinary Euclidean space $\mathbb{R}^3$,

$$\vec{r} : I \subseteq \mathbb{R} \longrightarrow \mathbb{R}^3, \tag{10}$$

passing through the centroids of the cross sections of the rod and where $s \in I$ is the arc-length parameter.

In order to describe the position of a generic cross section, it is useful to introduce a generalized orthonormal Frenet frame $\{\vec{d}_1(s), \vec{d}_2(s), \vec{d}_3(s)\}$, where $\vec{d}_1(s)$ and $\vec{d}_2(s)$ define the plane of the transverse section and $\vec{d}_3(s)$ is tangent to the curve $\vec{r}(s)$ under the assumption of unshearability. The variation of the $\vec{d}_i(s)$'s, $i = 1, 2, 3$ with respect to the arc-length is given in terms of the Darboux vector $\vec{k}(s)$:

$$\vec{k}(s) = \sum_{i=1}^{3} k_i(s)\vec{d}_i(s), \tag{11}$$

where $k_1(s)$ and $k_2(s)$ are associated with the bending and $k_3(s)$ to the torsion, in such a way that

$$\frac{\mathrm{d}\vec{d}_i(s)}{\mathrm{d}s} = \vec{k}(s) \times \vec{d}_i(s), \qquad i = 1, 2, 3. \tag{12}$$

For all $s \in I$, it is possible to define the Frenet basis $\{\vec{N}(s), \vec{B}(s), \vec{T}(s)\}$ constituted by the normal, binormal and tangent vectors to the curve $\vec{r}(s)$. The generalized and the usual Frenet frame are related by a rotation of an angle $\varphi(s)$ around $\vec{d}_3(s)$:

$$\begin{cases} \vec{d}_1(s) = \cos\varphi(s)\,\vec{N}(s) + \sin\varphi(s)\,\vec{B}(s) \\ \vec{d}_2(s) = -\sin\varphi(s)\,\vec{N}(s) + \cos\varphi(s)\,\vec{B}(s) \\ \vec{d}_3(s) = \vec{T}(s). \end{cases} \tag{13}$$

Following the terminology introduced in the study of DNA [16], we denote the angle $\varphi(s)$ as the *register*. We recall that, under the assumptions of unshearability and unexstensibility, the geometric configuration of the elastic rod is completely described once the components of the Darboux vector $\vec{k}(s)$ are assigned:

$$\begin{cases} k_1(s) = \kappa(s)\sin\varphi(s) \\ k_2(s) = \kappa(s)\cos\varphi(s) \\ k_3(s) = \tau(s) + \dfrac{\mathrm{d}\varphi(s)}{\mathrm{d}s}, \end{cases} \tag{14}$$

where

$$\kappa(s) = \left|\frac{\mathrm{d}\vec{T}(s)}{\mathrm{d}s}\right| \qquad \text{and} \qquad \tau(s) = -\frac{1}{\kappa(s)}\frac{\mathrm{d}\vec{T}(s)}{\mathrm{d}s}\cdot\frac{\mathrm{d}\vec{B}(s)}{\mathrm{d}s} \tag{15}$$

are, respectively, the curvature and the torsion of $\vec{r}(s)$, assumed to be functions of s, while $\frac{\mathrm{d}\varphi(s)}{\mathrm{d}s}$ is the *intrinsic twist*, that is a measure of the difference between the twist density and the Frenet torsion, see [6].

In the absence of external momenta and in the presence of an external load

$$\vec{f}(s) = \sum_{i=1}^{3} f_i(s)\vec{d}_i(s), \tag{16}$$

at the equilibrium, we obtain the static Kirchhoff equations

$$\begin{cases} \dfrac{\mathrm{d}\vec{F}(s)}{\mathrm{d}s} + \vec{f}(s) = 0 \\ \dfrac{\mathrm{d}\vec{M}(s)}{\mathrm{d}s} + \vec{d}_3(s) \times \vec{F}(s) = 0, \end{cases} \tag{17}$$

which involve the resultant of elastic stresses

$$\vec{F}(s) = \sum_{i=1}^{3} F_i(s)\vec{d}_i(s)$$

and the resultant torque

$$\vec{M}(s) = \sum_{i=1}^{3} M_i(s)\vec{d}_i(s)$$

acting on the cross section at $\vec{r}(s)$.

The torque $\vec{M}(s)$ is related to the strain variables by the following relationship:

$$\vec{M}(s) = a_1(s)k_1(s)\vec{d}_1(s) + a_2(s)k_2(s)\vec{d}_2(s) + b(s)k_3(s)\vec{d}_3(s), \tag{18}$$

where the functions $a_1(s)$ and $a_2(s)$ are the bending stiffnesses and are a measure of the asymmetry of the cross section, whereas $b(s)$ is the torsional stiffness, that is the response of the rod to the twist stress, see [9]. It is worth noting that these three quantities, when regarded as functions of the arc-length s, must be real, positive and bounded.

Projecting equations (17) in the $\{\vec{d}_i(s)\}_i$'s frame and using (18), we obtain the Kirchhoff system for the six unknowns (k_1, k_2, k_3) and (F_1, F_2, F_3), regarded as functions of the arc-length s:

$$\begin{cases} F_1' + k_2F_3 - k_3F_2 + f_1 = 0 \\ F_2' + k_3F_1 - k_1F_3 + f_2 = 0 \\ F_3' + k_1F_2 - k_2F_1 + f_3 = 0 \\ F_2 + (a_2 - b)k_2k_3 - a_1k_1' - k_1a_1' = 0 \\ F_1 + (a_1 - b)k_1k_3 + a_2k_2' + k_2a_2' = 0 \\ k_3'b + k_3b' - (a_1 - a_2)k_1k_2 = 0. \end{cases} \tag{19}$$

The energy density corresponding to a thin elastic rod described by (19) (see [6, 17–20]) is given by

$$\mathcal{E} = \tfrac{1}{2}\left[a_1k_1^2 + a_2k_2^2 + bk_3^2\right] + F_3. \tag{20}$$

The first term in (20) is the contribution due to bending and torsional deformations, while the last term is due to the presence of body forces along the rod. It is important to observe that $\mathcal{E}$ has the physical dimensions of an energy per unit of length, namely the dimensions of a force.

For the helical configuration described by (1) and under the assumption $\kappa \neq 0$, the total deformation energy is

$$E = \int_{-\infty}^{\infty} \mathcal{E}\,\mathrm{d}s, \tag{21}$$

keeping into account the translation invariance with respect to the arc-length s of equations (19). For a detailed treatment of the case $\kappa = 0$, we refer the reader to [10].

4. Inverse problem approach

Since most of the polymers we are interested in (i.e. α-helices, 3_{10}-helices, β-strands, etc) are folded as circular helices, in the following we will concern ourselves with circular helical solutions of (19). We recall that a circular helix is characterized by a constant curvature, torsion and, hence, constant pitch. Furthermore, in this paper we focus on the vanishing intrinsic twist case, namely we set $\varphi(s) = \varphi_0$.

Similarly to [9], we formulate the following inverse problem: we assign constant values to $\kappa(s)$ and $\tau(s)$:

$$\kappa(s) \equiv \kappa, \qquad \tau(s) \equiv \tau, \tag{22}$$

and solve (19) for the six unknowns $a_1(s), a_2(s), b(s), F_1(s), F_2(s), F_3(s)$, with assigned initial conditions at a specific value $s_0 \in I$ of the arc-length. Since all the equations in (19) are autonomous and invariant under translation with respect to s, here on we set $s_0 = 0$.

The long-range interacting model so far introduced can be regarded as a good approximation of those physical configurations featuring a constant register, since the force vectors describing the long-range interaction are placed on the centroids of the cross sections. In contrast, if the register varies with the arc-length, the hypothesis of neglecting the physical dimensions of the cross section (which allows us to approximate the interaction of the boundaries of the cross sections with the interaction of the corresponding centroids) is generally no longer valid. In this paper we mainly focus on the constant register case, postponing the detailed analysis of non-vanishing intrinsic twist to future works. It is worth noting that setting the register $\varphi(s) = \varphi_0$ entails, via (22), that (19) is a system of linear ODEs in the six unknowns $a_1(s), a_2(s), b(s), F_1(s), F_2(s), F_3(s)$, whose solutions are presented below, following the classification scheme introduced in [9].

4.1. Constant register solution for $\tau \neq 0$ and $\kappa \neq 0$

If the curvature and the torsion are different from zero, then the helix is non-degenerate. From parametrization (1), we obtain that

$$\kappa = \frac{r}{r^2 + c^2} \qquad \text{and} \qquad \tau = \frac{c}{r^2 + c^2}. \tag{23}$$

It is expedient to split this case into three subcases, depending on whether φ is an (even or odd) integer multiple of $\frac{\pi}{2}$ or not.

4.1.1. $\varphi(s) \equiv \frac{\pi}{2} + n\pi, n \in \mathbb{Z}$. Under this assumption the solution of (19) reads as follows:

$$\begin{cases} a_1(s) = a_0 \\ a_2(s) \in \mathcal{C}^1(\mathbb{R}) \\ b(s) = b_0 \end{cases} \tag{24a}$$

$$\begin{cases} k_1(s) = (-1)^n \dfrac{r}{c^2 + r^2} \\ k_2(s) = 0 \\ k_3(s) = \dfrac{c}{c^2 + r^2} \end{cases} \tag{24b}$$

$$\begin{cases} F_1(s) = (-1)^n \dfrac{cr}{(c^2 + r^2)^2} (b_0 - a_0) \\ F_2(s) = 0 \\ F_3(s) = \dfrac{c^2}{(c^2 + r^2)^2} (b_0 - a_0) + (-1)^n \left(\dfrac{c^2}{r} + r \right) f_2, \end{cases} \tag{24c}$$

where f_1, f_2 and f_3 are the components of the load vector, as in (16), f_2 is constant and f_1 and f_3 satisfy the following condition:

$$\begin{cases} f_1 = 0 \\ f_3 = 0. \end{cases} \tag{24d}$$

We recall that $a_0 = a_1(0)$ and $b_0 = b(0)$ are arbitrary real positive constants. Furthermore, $a_2(s)$ is an arbitrary real positive smooth function of the arc-length s.

In this case it is important to underline that (24*d*) entails that the integrability of (19) is guaranteed only if the vector $\vec{f}$ features a single component along $\vec{N}$, as can be easily seen by recalling that setting $\varphi = \frac{\pi}{2} + n\pi$, via (13), implies $\vec{d}_1 = (-1)^n \vec{B}$ and $\vec{d}_2 = (-1)^{n+1} \vec{N}$. This is indeed the case of the load vector $\vec{f}$ described in (8*a*)–(8*b*) and (9).

Via (20) the elastic energy density is

$$\mathcal{E} = \frac{a_0 r^2 + (3b_0 - 2a_0)c^2}{2\left(c^2 + r^2\right)^2} + (-1)^n \left(r + \frac{c^2}{r}\right) f_2, \tag{25}$$

where we recall that f_2 generally might depend on r and c.

4.1.2. $\varphi(s) \equiv n\pi, n \in \mathbb{Z}$. Under this assumption the solution of (19) reads as follows:

$$\begin{cases} a_1(s) \in \mathcal{C}^1(\mathbb{R}) \\ a_2(s) = a_0 \\ b(s) = b_0 \end{cases} \tag{26a}$$

$$\begin{cases} k_1(s) = 0 \\ k_2(s) = (-1)^n \dfrac{r}{c^2 + r^2} \\ k_3(s) = \dfrac{c}{c^2 + r^2} \end{cases} \tag{26b}$$

$$\begin{cases} F_1(s) = 0 \\ F_2(s) = (-1)^n \dfrac{cr}{(c^2 + r^2)^2} (b_0 - a_0) \\ F_3(s) = \dfrac{c^2}{(c^2 + r^2)^2} (b_0 - a_0) + (-1)^{n+1} \left(\dfrac{c^2}{r} + r\right) f_1 \end{cases} \tag{26c}$$

with the condition

$$\begin{cases} f_2 = 0 \\ f_3 = 0. \end{cases} \tag{26d}$$

We recall that $a_0 = a_2(0)$ and $b_0 = b(0)$ are arbitrary real positive constants. Furthermore, $a_1(s)$ is an arbitrary real positive smooth function of the arc-length s.

In this case it is important to underline that (26*d*) entails that the integrability of (19) is guaranteed only if the vector $\vec{f}$ features a single component along $\vec{N}$, as can be easily seen by recalling that setting $\varphi = n\pi$, via (13), implies $\vec{d}_1 = (-1)^n \vec{N}$ and $\vec{d}_2 = (-1)^n \vec{B}$. This is indeed the case of the load vector $\vec{f}$ described in (8*a*)–(8*b*) and (9).

Via (20) the elastic energy density is

$$\mathcal{E} = \frac{a_0 r^2 + (3b_0 - 2a_0)c^2}{2(c^2 + r^2)^2} + (-1)^{n+1} \left(r + \frac{c^2}{r}\right) f_1, \tag{27}$$

where we recall that f_1 generally might depend on r and c.

4.1.3. $\varphi(s) \equiv \varphi_0 \neq n\,\frac{\pi}{2}$, $n \in \mathbb{Z}$. Under this assumption, the solution of (19) reads as follows:

$$\begin{cases} a_1(s) = a_0 - 2\beta_0\left(1+\dfrac{c^2}{r^2}\right)\left[c\cos\left(\dfrac{s}{\sqrt{c^2+r^2}}\right) + \sqrt{c^2+r^2}\,\cot(\varphi_0)\sin\left(\dfrac{s}{\sqrt{c^2+r^2}}\right)\right] \\ a_2(s) = a_0 - 2\beta_0\left(1+\dfrac{c^2}{r^2}\right)\left[c\cos\left(\dfrac{s}{\sqrt{c^2+r^2}}\right) + \sqrt{c^2+r^2}\,\tan(\varphi_0)\sin\left(\dfrac{s}{\sqrt{c^2+r^2}}\right)\right] \\ b(s) = b_0 + 2\beta_0\left(c+\dfrac{r^2}{c}\right)\cos\left(\dfrac{s}{\sqrt{c^2+r^2}}\right) \end{cases} \tag{28a}$$

$$\begin{cases} k_1(s) = \dfrac{r}{c^2+r^2}\sin(\varphi_0) \\ k_2(s) = \dfrac{r}{c^2+r^2}\cos(\varphi_0) \\ k_3(s) = \dfrac{c}{c^2+r^2} \end{cases} \tag{28b}$$

$$\begin{cases} F_1(s) = \dfrac{cr}{c^2+r^2}(b_0-a_0)\sin(\varphi_0) \\ F_2(s) = \dfrac{cr}{c^2+r^2}(b_0-a_0)\cos(\varphi_0) \\ F_3(s) = \dfrac{c^2}{(c^2+r^2)^2}(b_0-a_0) - \left(r+\dfrac{c^2}{r}\right)f, \end{cases} \tag{28c}$$

where f_1, f_2 and f_3 are the components of the load vector, as in (16), and satisfy the following condition:

$$\begin{cases} f_1 = f\cos(\varphi_0) \\ f_2 = -f\sin(\varphi_0) \\ f_3 = 0. \end{cases} \tag{28d}$$

Here a_0, b_0 and β_0 are real integration constants that satisfy the conditions

$$\begin{cases} a_0 > 2\beta_1\left(1+\dfrac{c^2}{r^2}\right)\max\left\{\sqrt{c^2+(c^2+r^2)\cot^2(\varphi_0)}, \sqrt{c^2+(c^2+r^2)\tan^2(\varphi_0)}\right\} \\ b_0 > 2\,\beta_0\left(c+\dfrac{r^2}{c}\right). \end{cases} \tag{28e}$$

In this case it is important to underline that (28*d*) entails that the integrability of (19) is guaranteed only if the vector $\vec{f}$ is parallel to $\vec{N}$, as can be easily seen by comparing (28*d*) with (13). This is indeed the case of the load vector $\vec{f}$ described in (8*a*)–(8*b*) and (9).

Via (20) the elastic energy density is

$$\mathcal{E} = \frac{a_0 r^2 + (3b_0 - 2a_0)c^2}{2(c^2+r^2)^2} - \left(r+\frac{c^2}{r}\right)f, \tag{29}$$

where we recall that f generally might depend on r and c.

4.2. Constant register solution for $\tau = 0$ *and* $\kappa \neq 0$

If the torsion vanishes, then the central line of the helix degenerates into a circle. From parametrization (1), we obtain that

$$\kappa = \frac{1}{r} \qquad \text{and} \qquad \tau = 0. \tag{30}$$

It is expedient to split this case into three subcases, depending on whether φ is an (even or odd) integer multiple of $\frac{\pi}{2}$ or not.

4.2.1. $\varphi(s) \equiv \frac{\pi}{2} + n\pi, n \in \mathbb{Z}$. Under this assumption the solution of (19) reads as follows:

$$\begin{cases} a_1(s) = r^2\left[\alpha_0 + \alpha_1 \cos\left(\frac{s}{r}\right) + \alpha_2 \sin\left(\frac{s}{r}\right) + (-1)^{n+1} r f_2\right] \\ a_2(s) \in \mathcal{C}^1(\mathbb{R}) \\ b(s) \in \mathcal{C}^1(\mathbb{R}) \end{cases} \tag{31a}$$

$$\begin{cases} k_1(s) = \dfrac{(-1)^n}{r} \\ k_2(s) = 0 \\ k_3(s) = 0 \end{cases} \tag{31b}$$

$$\begin{cases} F_1(s) = 0 \\ F_2(s) = (-1)^{n+1}\left[\alpha_1 \sin\left(\frac{s}{r}\right) - \alpha_2 \cos\left(\frac{s}{r}\right)\right] \\ F_3(s) = -\left[\alpha_1 \cos\left(\frac{s}{r}\right) + \alpha_2 \sin\left(\frac{s}{r}\right)\right] + (-1)^n r f_2, \end{cases} \tag{31c}$$

where f_1, f_2 and f_3 are the components of the load vector, as in (16), f_2 is constant and f_1 and f_3 satisfy the following condition:

$$\begin{cases} f_1 = 0 \\ f_3 = 0. \end{cases} \tag{31d}$$

We recall that the constants appearing in (31*a*)–(31*c*) must satisfy the condition $\alpha_0 + (-1)^{n+1} r f_2 > \sqrt{\alpha_1^2 + \alpha_2^2}$. Furthermore, $a_2(s)$ and $b(s)$ are arbitrary real positive smooth functions of the arc-length s.

In this case it is important to underline that (31*d*) entails that the integrability of (19) is guaranteed only if the vector $\vec{f}$ features a single component along $\vec{N}$, as can be easily seen by recalling that setting $\varphi = \frac{\pi}{2} + n\pi$, via (13), implies $\vec{d}_1 = (-1)^n \vec{B}$ and $\vec{d}_2 = (-1)^{n+1} \vec{N}$. This is indeed the case of the load vector $\vec{f}$ described in (8*a*)–(8*b*) and (9).

Via (20) the elastic energy density is

$$\mathcal{E} = \frac{1}{2}\left[\alpha_0 - \alpha_1 \cos\left(\frac{s}{r}\right) - \alpha_2 \sin\left(\frac{s}{r}\right) + (-1)^n r f_2\right], \tag{32}$$

where we recall that f_2 generally might depend on r and c.

4.2.2. $\varphi(s) \equiv n\pi, n \in \mathbb{Z}$. Under this assumption, the solution of (19) reads as follows:

$$\begin{cases} a_1(s) \in \mathcal{C}^1(\mathbb{R}) \\ a_2(s) = r^2\left[\alpha_0 + \alpha_1 \cos\left(\frac{s}{r}\right) + \alpha_2 \sin\left(\frac{s}{r}\right) + (-1)^n r f_1\right] \\ b(s) \in \mathcal{C}^1(\mathbb{R}) \end{cases} \tag{33a}$$

$$\begin{cases} k_1(s) = 0 \\ k_2(s) = \frac{(-1)^n}{r} \\ k_3(s) = 0 \end{cases} \tag{33b}$$

$$\begin{cases} F_1(s) = (-1)^n\left[\alpha_1 \sin\left(\frac{s}{r}\right) - \alpha_2 \cos\left(\frac{s}{r}\right)\right] \\ F_2(s) = 0 \\ F_3(s) = -\left[\alpha_1 \cos\left(\frac{s}{r}\right) + \alpha_2 \sin\left(\frac{s}{r}\right)\right] + (-1)^{n+1} r f_1 \end{cases} \tag{33c}$$

with the condition

$$\begin{cases} f_2 = 0 \\ f_3 = 0. \end{cases} \tag{33d}$$

We recall that the constants appearing in (33*a*)–(33*c*) must satisfy the condition $\alpha_0 + (-1)^n r f_1 > \sqrt{\alpha_1^2 + \alpha_2^2}$. Furthermore, $a_1(s)$ and $b(s)$ are arbitrary real positive smooth functions of the arc-length s.

In this case it is important to underline that (33*d*) entails that the integrability of (19) is guaranteed only if the vector $\vec{f}$ features a single component along $\vec{N}$, as can be easily seen by recalling that setting $\varphi = n\pi$, via (13), implies $\vec{d}_1 = (-1)^n \vec{N}$ and $\vec{d}_2 = (-1)^n \vec{B}$. This is indeed the case of the load vector $\vec{f}$ described in (8*a*)–(8*b*) and (9).

Via (20) the elastic energy density is

$$\mathcal{E} = \frac{1}{2}\left[\alpha_0 - \alpha_1 \cos\left(\frac{s}{r}\right) - \alpha_2 \sin\left(\frac{s}{r}\right) + (-1)^{n+1} r f_1\right], \tag{34}$$

where we recall that f_1 generally might depend on r and c.

4.2.3. $\varphi(s) \equiv \varphi_0 \neq n\frac{\pi}{2}, n \in \mathbb{Z}$. Under this assumption the solution of (19) reads as follows:

$$\begin{cases} a_1(s) = r^2\left[\alpha_0 - \alpha_1 \cos\left(\frac{s}{r}\right) - \alpha_2 \sin\left(\frac{s}{r}\right) + rf\right] \\ a_2(s) = r^2\left[\alpha_0 - \alpha_1 \cos\left(\frac{s}{r}\right) - \alpha_2 \sin\left(\frac{s}{r}\right) + rf\right] \\ b(s) \in \mathcal{C}^1(\mathbb{R}) \end{cases} \tag{35a}$$

$$\begin{cases} k_1(s) = \dfrac{\sin(\varphi_0)}{r} \\ k_2(s) = \dfrac{\cos(\varphi_0)}{r} \\ k_3(s) = 0 \end{cases} \tag{35b}$$

$$\begin{cases} F_1(s) = -\cos(\varphi_0)\left[\alpha_1 \sin\left(\frac{s}{r}\right) - \alpha_2 \cos\left(\frac{s}{r}\right)\right] \\ F_2(s) = \sin(\varphi_0)\left[\alpha_1 \sin\left(\frac{s}{r}\right) - \alpha_2 \cos\left(\frac{s}{r}\right)\right] \\ F_3(s) = \alpha_1 \cos\left(\frac{s}{r}\right) + \alpha_2 \sin\left(\frac{s}{r}\right) - rf, \end{cases} \tag{35c}$$

where f_1, f_2 and f_3 are the components of the load vector, as in (16), and satisfy the following condition:

$$\begin{cases} f_1 = f\cos(\varphi_0) \\ f_2 = -f\sin(\varphi_0) \\ f_3 = 0. \end{cases} \tag{35d}$$

We recall that the constants appearing in (35*a*)–(35*c*) must satisfy the condition $\alpha_0 + rf > \sqrt{\alpha_1^2 + \alpha_2^2}$. Furthermore, $b(s)$ is an arbitrary real positive smooth function of the arc-length s.

In this case it is important to underline that (35*d*) entails that the integrability of (19) is guaranteed only if the vector $\vec{f}$ is parallel to $\vec{N}$, as can be easily seen by comparing (35*d*) with (13). This is indeed the case of the load vector $\vec{f}$ described in (8*a*)–(8*b*) and (9).

Via (20) the elastic energy density is

$$\mathcal{E} = \frac{1}{2}\left[\alpha_0 + \alpha_1 \cos\left(\frac{s}{r}\right) + \alpha_2 \sin\left(\frac{s}{r}\right) - rf\right], \tag{36}$$

where we recall that f generally might depend on r and c.

4.3. Constant register solution for $\tau = 0$ and $\kappa = 0$

If the torsion and the curvature vanish, then the central line of the helix degenerates into a straight line.

The explicit solution of (19) reads as follows:

$$\begin{cases} a_1(s) \in \mathcal{C}^1(\mathbb{R}) \\ a_2(s) \in \mathcal{C}^1(\mathbb{R}) \\ b(s) \in \mathcal{C}^1(\mathbb{R}) \end{cases} \tag{37a}$$

$$\begin{cases} k_1(s) = 0 \\ k_2(s) = 0 \\ k_3(s) = 0 \end{cases} \tag{37b}$$

$$\begin{cases} F_1(s) = 0 \\ F_2(s) = 0 \\ F_3(s) \in \mathcal{C}^1(\mathbb{R}) \end{cases} \tag{37c}$$

with the condition

$$\begin{cases} f_1 = 0 \\ f_2 = 0 \\ f_3 = 0. \end{cases} \tag{37d}$$

We recall that $a_1(s)$, $a_2(s)$, $b(s)$ and $F_3(s)$ are arbitrary real positive smooth functions of the arc-length s.

In this case it is important to underline that (37*d*) entails that the integrability of (19) is guaranteed only if the vector $\vec{f}$ vanishes.

Formula (20) entails that the elastic energy density equals $F_3(s)$.

5. The external force behavior

It is well known that, in the absence of strong electrostatic effects, long-range interactions related to dispersion forces tune the behavior of polymeric chains. Although they are usually expressed by Lennard-Jones potentials, a Morse-type potential has greater flexibility and 'softer' boundary conditions (see [21]). We then derive the modulus of $\Phi(x)$, see (4), from the following Morse-type potential:

$$V(x) = D_0[\mathrm{e}^{-\alpha(x-x_0)} - 1]^2 + V_0, \tag{38}$$

where x is the distance between two interacting points, x_0 is the equilibrium distance, $D_0 > 0$ is the so-called well depth, $\alpha > 0$ is an opportune-dimensional parameter linked to the force constant at the equilibrium and $V_0 = V(x_0) - D_0$, see [22].

For such a potential, the integral in (8*b*) is well defined and the force derived from (38) via (4) is

$$\Phi(x) = 2\alpha D_0\, \mathrm{e}^{-\alpha(x-x_0)}[\mathrm{e}^{-\alpha(x-x_0)} - 1], \tag{39}$$

which is strongly repulsive—though not diverging—for vanishing distance between two interacting points of the rod.

The integral in (8*b*) cannot be achieved analytically in a closed form, nevertheless we prove its convergence for $c \neq 0$ providing an explicit evaluation of its modulus:

$$\begin{aligned} |\mathcal{F}| &\leqslant 2r \int_0^\infty \left| \frac{1-\cos(t)}{X(t)}\, \Phi(X(t)) \right| \mathrm{d}t \\ &\leqslant 4\alpha D_0 r \int_0^\infty \frac{1-\cos t}{ct}\, \mathrm{e}^{2\alpha(x_0-ct)}\, \mathrm{d}t \\ &= \frac{2\alpha D_0 r}{c}\, \mathrm{e}^{2\alpha x_0}\, \ln\left[1+\frac{1}{4\alpha^2 c^2}\right]. \end{aligned} \tag{40}$$

Note that the last right-hand side of (40) is finite if $c \neq 0$.

If c approaches zero, the integral in (8*b*) may diverge. For instance, when $\varphi = \frac{\pi}{2}$, by evaluating the limit of (25) as $c \to 0$ we get

$$\begin{aligned} &\mathcal{E} = \frac{a_0}{2r^2} + \lim_{m\in\mathbb{N},\, m\to\infty} 16\, m\, \pi\alpha D_0\, \mathrm{e}^{\alpha x_0}\, g(\alpha, r, x_0), \\ &g(\alpha, r, x_0) = L_{-1}(2\alpha r) - I_1(2\alpha r) - \mathrm{e}^{\alpha x_0}[L_{-1}(4\alpha r) - I_1(4\alpha r)], \end{aligned} \tag{41}$$

which is evidently plus or minus infinity whether the bounded quantity $g(\alpha, r, x_0)$ is strictly positive or negative, respectively (when $g(\alpha, r, x_0) = 0$ then the limit of (25) as $c \to 0$ is not defined). We recall that in (41) $L_{-1}(x)$ is the Struve function L of order -1 and $I_1(x)$ is the Bessel function I of order 1. Moreover, it is important to observe that (41) is formally different from (32) which is an arc-length-dependent quantity; the reason of this difference lies into the fact that setting $c = 0$ first and then solving the inverse problem illustrated in section 4 is clearly not equivalent to solving equations (19) for $c \neq 0$ and then setting $c = 0$.

If c approaches infinity, the energy density (25) approaches zero for fixed values of $r \neq 0$.

If r approaches zero, the energy density (20) is always finite, but can depend on the arc-length in the degenerate cases depicted in sections 4.2–4.3. For instance, when $\varphi = \frac{\pi}{2}$, by evaluating the limit of (25) as $r \to 0$, we get

$$\mathcal{E} = \frac{3b_0 - 2a_0}{2c^2} - 4\alpha D_0\, \mathrm{e}^{\alpha x_0} \left[\mathrm{e}^{\alpha x_0}\, \ln\left(1+\frac{1}{4c^2\alpha^2}\right) - \ln\left(1+\frac{1}{c^2\alpha^2}\right)\right]. \tag{42}$$

If r approaches infinity, the energy density (25) approaches zero for fixed values of $c \neq 0$.

In order to discuss non-degenerate helical configurations of elastic rods as a model for polymeric chains, it is mandatory to underline that vanishing values of c and/or r are not physically relevant.

6. Elastic energy for non-degenerate circular helical configurations

In this section we show that, for typical values of the parameters of the Morse potential (38) which describes the two-point intra-chain interactions appearing in a polypeptide in α-helix configuration, the energy density can feature stationary points with respect to the radius and pitch of the helix. Such intra-chain interactions are possibly due to the formation of different kinds of non-bonding hydrogen bonds among non-contiguous elements of the polymeric chain, such as the $\mathrm{N-H\cdots O=C}$ interaction among amidic sites and/or the $\mathrm{CH_3\cdots CH_3}$ interaction among methyl sites.

We start by discussing the energy densities determined in section 4. Thus, it is mandatory to underline that in our analysis we implicitly constrain the elastic rod to take only circular helical configurations, so that the stationary points given below do not represent global equilibrium among all possible configurations.

We recall that (see [17, 19]), for an isotropic homogeneous rod whose curvature and torsion are non-vanishing, the bending stiffnesses are $a_1(s) = YI_1$ and $a_2(s) = YI_2$, and the torsional stiffness is $b(s) = \mu J$, where Y and μ are respectively the Young and shear moduli (which are intrinsic characteristics of the material), while I_1, I_2 and J are the geometrical momenta of inertia (which depend on the shape of the cross section of the backbone). For the sake of simplicity, if we assume that $\varphi = \frac{\pi}{2}$, then the bending stiffnesses are equal and constant, namely $a_1(s) = a_2(s) = a_0$, and the torsional stiffness is constant, namely $b(s) = b_0$, as displayed in (24*a*); therefore, the compatible cross section shapes are those which feature $I_1 = I_2 = I$. It is well known that for a circle and for every regular polygon, the moment of inertia I with respect to every axis through the centroid (as the principal axes) is the same. For such shapes we get

$$a_0 = YI \qquad \text{and} \qquad b_0 = \mu J. \tag{43}$$

For instance, if the cross section of the backbone of the polymer is assumed to be circular and ℓ is the length of its diameter, then we have (see [19])

$$I = \frac{\pi}{4}\ell^4 \qquad \text{and} \qquad J = \frac{\pi}{2}\ell^4; \tag{44a}$$

if the cross section is assumed to be a square and ℓ is the length of its edge, then we have

$$I = \frac{\ell^4}{12} \qquad \text{and} \qquad J = \frac{\ell^4}{6}; \tag{44b}$$

if the cross section is assumed to be an equilateral triangle and ℓ is the length of its edge, then we have

$$I = \frac{\sqrt{3}}{96}\,\ell^4 \qquad \text{and} \qquad J = \frac{\sqrt{3}}{48}\,\ell^4. \tag{44c}$$

In the following, and unless otherwise specified, we mainly focus on polymers featuring a circular cross section (44*a*). Let us consider the specific case of polyalanine, a homopolymer of the simplest chiral aminoacid L-alanine. The average value of ℓ for such a polypeptide is 3×10^{-10} m, see [22, 23].

Ab initio molecular dynamics simulations and force field (FFs) computations (see [24, 25]) indicate that, for the intra-chain interactions described above, values for the Morse parameters D_0, α and x_0 appearing in (38) can be chosen to span from

$$D_0 = 4.58 \times 10^{-21}\,\mathrm{J} \qquad \alpha = 1.4 \times 10^{10}\,\mathrm{m}^{-1} \qquad x_0 = 1.6 \times 10^{-10}\,\mathrm{m}, \tag{45a}$$

which correspond to the weak H bond due to the amidic $\mathrm{N-H\cdots O=C}$ interactions, see [24], to

$$D_0 = 1.13 \times 10^{-18}\,\mathrm{J} \qquad \alpha = 1.8 \times 10^{10}\,\mathrm{m}^{-1} \qquad x_0 = 0.8 \times 10^{-10}\,\mathrm{m}, \tag{45b}$$

which correspond to the strong H bond due to the methyl $\mathrm{CH_3\cdots CH_3}$ interactions, see [25].

Furthermore, for a polyalanine α-helix, the following elastic moduli have been computed by atomistic simulations [26]:

$$Y = 2.50 \times 10^9\,\mathrm{J\,m^{-3}} \qquad \text{and} \qquad \mu = 0.91 \times 10^9\,\mathrm{J\,m^{-3}}. \tag{46}$$

It is mandatory to recall here that values of the Young and shear moduli similar to those reported in (46), as well as values of the Morse parameters similar to those reported in (45*a*) and (45*b*), do apply for a wider class of polypeptides than the simple polyalanine molecule herein considered. As a consequence of (46), via (43) and (44*a*), for a circular shape of the backbone, the stiffnesses are

$$a = 1.71 \times 10^{-29}\,\mathrm{J\,m} \qquad \text{and} \qquad b = 1.24 \times 10^{-29}\,\mathrm{J\,m}, \tag{47}$$

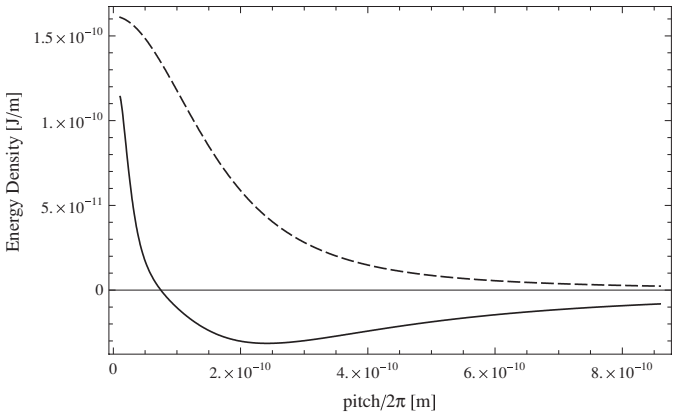

Figure 3. Energy density $\mathcal{E}$ (J m^{-1}) vs c (m) in the presence (solid) and in the absence (dashed) of a long-range interaction (39) with D_0, α and x_0 as in (45*a*).

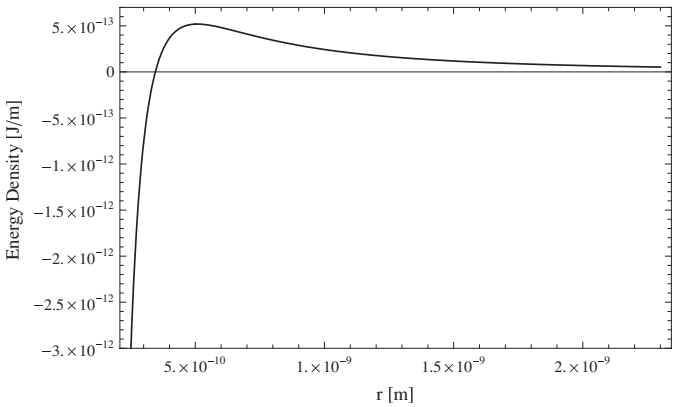

Figure 4. Energy density $\mathcal{E}$ (J m^{-1}) vs r [m] in the presence of a long-range interaction (39) with D_0, α and x_0 as in (45*a*).

and the typical values of radius and pitch for an α-helix are respectively

$$r = 0.23 \times 10^{-9}\,\mathrm{m} \qquad \text{and} \qquad p = 2\pi c = 0.54 \times 10^{-9}\,\mathrm{m}. \tag{48}$$

As a result, by integrating numerically (25), via (38), we obtain the energy density landscapes depicted in figures 3–6. Numerical integrations were performed through an adaptive Gaussian quadrature algorithm [27].

Figures 3 and 5 show the energy density $\mathcal{E}$ vs c, with $\varphi = \frac{\pi}{2}$ (see (25)), $a_0 = a$, $b_0 = b$, $r = 0.23 \times 10^{-9}$ m (see (48)) and the Morse parameters as in (45*a*) and (45*b*) respectively. In both figures we compare the two cases corresponding to the presence and to the absence (namely setting $D_0 = 0$, see [10]) of the long-range interaction (38). From (47) we get $\frac{a}{b} < \frac{3}{2}$ and, as proved in [10] in the absence of long-range interactions, this condition verifies no local minima for the energy density. Therefore, the observed local minima are uniquely due to the presence of the intra-chain long-range interaction potential. Moreover, the fact that we observe those minima at both the extremes of the range (45*a*)–(45*b*) suggests that one might observe

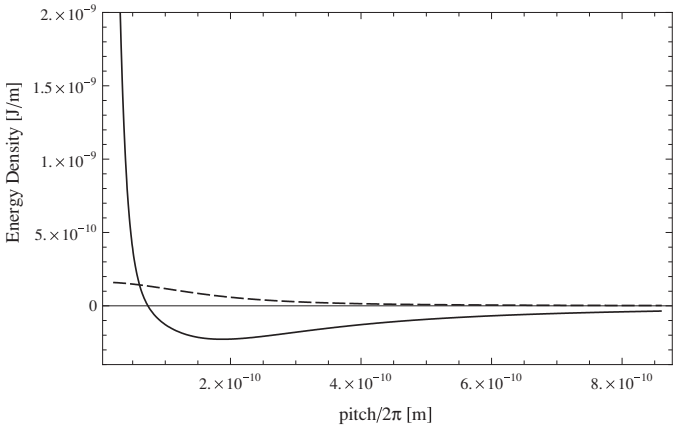

Figure 5. Energy density $\mathcal{E}$[J/m] vs c [m] in the presence (solid) and in the absence (dashed) of a long-range interaction (39) with D_0, α and x_0 as in (45*b*).

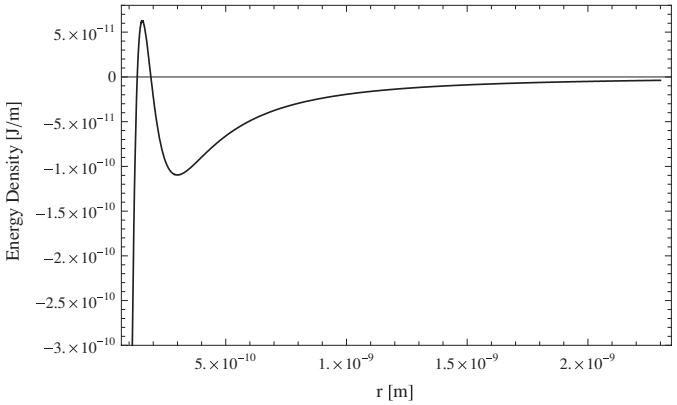

Figure 6. Energy density $\mathcal{E}$[J/m] *vs* r [m] in the presence of a long-range interaction (39) with D_0, α and x_0 as in (45*b*).

them also for all values in the range. The existence of such minima entails the existence of stable helical configurations for the polymer folding under the assumption of fixed radius.

Figures 4 and 6 show the energy density $\mathcal{E}$ vs r when $c = 0.86 \times 10^{-11}$ m as in (48) and the Morse parameters are as in (45*a*) and (45*b*) respectively. We recall that, as $r \to 0$, the energy density $\mathcal{E}$ has a finite limit, see (42). In figure 4, $\mathcal{E}$ features a local maximum and, as $r \to \infty$, the energy density approaches monotonically zero from above, while in figure 6, $\mathcal{E}$ features first a local maximum and then a minimum before converging monotonically to zero from below for large values of r. We recall that the maxima depicted in figures 4 and 6 represent unstable helical foldings of the polymer, while the minimum in figure 6 entails the existence of a stable helical configuration, under the assumption of fixed pitch.

As a final remark, we discuss numerically the role played by the shape of the cross section of the backbone of the polymeric chain on the energy density landscape. In figure 7 we show the energy density $\mathcal{E}$ vs c when $r = 0.23 \times 10^{-9}$ m as in (48) and the Morse parameters are as in (45*b*). Three different curves are presented, corresponding to three different choices of

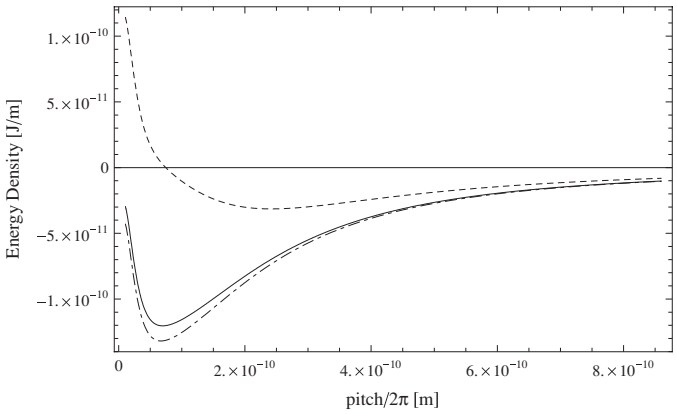

Figure 7. Energy density $\mathcal{E}$ (J m^{-1}) vs c (m) in the presence of a long-range interaction (39) with D_0, α and x_0 as in (45*b*) for different shapes of the cross-section of the rod: circular (dashed), squared (solid) and triangular (point-dashed).

the cross section shape: circular, squared and triangular. Elastic rods as models for polymeric chains, whose backbone is mapped into a polygonal cross section, seem to have lower values of the energy density if the number of edges decreases. For instance, with the choice (45*b*), the difference of the minima of the energy density between the circular and the triangular cross sections is of the order of 1×10^{-10} J m^{-1}.

7. Conclusions and perspectives

In the present paper we showed that the static Kirchhoff equations for an elastic rod in the presence of an external force are integrable, indeed solvable, if the central line of the rod is assumed to be helical and the external force is constant in modulus and directed as the normal vector to the central line. Such an external force can be obtained by averaging a long-range interaction between all the points of the central line for a rod of infinite length. We established and solved an inverse problem to determine the physical parameters characterizing the elastic properties of the rod in the case of a constant register (vanishing intrinsic twist) once the geometrical parameters of the helix have been fixed. We postpone the study of the case of non-vanishing intrinsic twist to future investigations. Moreover, we studied the elastic energy densities with respect to the radius and pitch of the helix, and we showed numerically the existence of stationary points, under the constraint of helical configurations, for plausible choices of the values of the parameters corresponding to a real polypeptide chain. These results were obtained from explicit analytical solutions of the (generalized) static Kirchhoff equations, without recurring to numerical simulations in order to infer the shape of the elastic rod. Despite the simplicity of the herein-treated model, which does not take into account many fundamental aspects of real macromolecular system (e.g. the presence of a reasonable solution fluid at a given temperature, or the effects of clamped extremes), we showed that a good qualitative agreement with some expected features of a given polypeptide is observed (for a comparison, see [12], where the authors discuss analytical and numerical results obtained through a different model).

It is left to be studied how to deal with rods of finite length since, in that case, the finite geometry compels the averaged force not to be constant both in modulus and direction as

much as one considers points closer to the extremes of the rod: taking into account such end effects seems to be an 'elusive computation', as already pointed out in [8]. Furthermore, in order to model real polymeric chains, in future studies it will be mandatory to focus on the overall energy of the elastic rod, including the presence of a fluid surrounding the rod by introducing thermal and cavitational terms in the free energy potential, see [28, 29]. It is our opinion that the analytical model discussed herein, when the above-mentioned physical and chemical constraints are opportunely taken into account, can play a fundamental role in the multiscale approach to polymers and bio-polymers, where a description at different space- and time-scales is needed.

Acknowledgments

The authors wish to thank Professor Vincenzo Barone for his critical reading of the manuscript and for enlightening discussions.

References

[1] D'Amore M, Talarico G and Barone V 2006 *J. Am. Chem. Soc.* **128** 1099
[2] Langella E, Improta R and Barone V 2004 *Biophys. J.* **87** 3623
[3] Gohlke H and Thorpe M F 2006 *Biophys. J.* **91** 2115
[4] Hafner J, Wolverton C and Ceder G 2006 *MRS Bull.* **31** 659
[5] Hammes-Schiffer S and Benkovic S J 2006 *Ann. Rev. Biochem.* **75** 519
[6] Goriely A, Nizette M and Tabor M 2001 *J. Nonlinear Sci.* **11** 3
[7] Dichmann D, Li Y and Maddocks J H 1996 *Hamiltonian Formulations and Symmetries in Rod Mechanics (Mathematical Approaches to Biomolecular Structure and Dynamics. IMA Vol. Math. Appl.* vol 82*)* (New York: Springer) pp 71–113
[8] Chouaieb N, Goriely A and Maddocks J H 2006 *Proc. Natl Acad. Sci.* **103** 9398
[9] Argeri M, Barone V, De Lillo S, Lupo G and Sommacal M 2009 *Physica* D **238** 1031
[10] Argeri M, Barone V, De Lillo S, Lupo G and Sommacal M 2009 *Theor. Math. Phys.* **159** 698
[11] Balaeff A, Mahadevan L and Schulten K 1999 *Phys. Rev. Lett.* **83** 4900
[12] Banavar J R, Hoang T X, Maddocks J H, Maritan A, Poletto C, Stasiak A and Trovato A 2007 *Proc. Natl Acad. Sci.* **104** 17283
[13] Goyal S, Perkins N C and Lee C L 2008 *Int. J. Non-Linear Mech.* **43** 65
[14] Postnikov M 1987 *Leçons de Géométrie. Variétés Différentiables* (Moscow: MIR)
[15] Antman S S 1995 *Nonlinear Problems of Elasticity* (New York: Springer)
[16] Kirchhoff G 1883 *Vorlesungen über Mathematische Physik: Mechanik* 3rd edn (Leipzig: Teubner)
[17] Love A E H 1926 *A Treatise on the Mathematical Theory of Elasticity* (New York: Dover)
[18] Sanghani S R, Zakrzewska K, Harvey S C and Lavery R 1996 *Nucl. Acids Res.* **24** 1632
[19] Bower A F 2008 *Applied Mechanics of Solids,* http://solidmechanics.org
[20] Coleman B D, Dill E H, Lembo M, Lu Z and Tobias I 1993 *Arch. Rational Mech. Anal.* **121** 339
[21] Abraham R J and Stölevik R 1978 *Chem. Phys. Lett.* **58** 622
[22] Atkins P W and De Paula J 2006 *Physical Chemistry* (Oxford: Oxford University Press)
[23] Meurer K P and Vögtle F 1985 *Top. Curr. Chem.* **127** 1
[24] Kang Y K 2000 *J. Phys. Chem. B* **104** 8321
[25] Amodeo P and Barone V 1992 *J. Am. Chem. Soc.* **114** 9085
[26] Hawkins R J and McLeish T C B 2006 *J. R. Soc. Interface* **3** 125
[27] Hildebrand F B 1956 *Introduction to Numerical Analysis* (New York: McGraw-Hill)
[28] Pierotti R A 1976 *Chem. Rev.* **76** 717
[29] Höfinger S and Zerbetto F 2003 *Chem. Eur. J.* **9** 566